Compact Dual-Polarized Shared-Dipole Antennas for Base Station Applications

Le-Hu Wen, Steven Gao, *Senior Member, IEEE*, Qi Luo, *Member, IEEE*, Chun-Xu Mao, *Member, IEEE*, Wei Hu, *Member, IEEE*, Yingzeng Yin, *Member, IEEE*, Yonggang Zhou, and Qiwei Wang

***Abstract*— Crossed-dipole (CD) antennas have been widely employed for dual polarization in wireless communication systems in recent years. In this paper, a novel design concept of dual-polarized shared-dipole (DPSD) antenna is presented. Different from the traditional CD antennas, the arms of the DPSD antenna are shared for two orthogonal polarizations. This design technique leads to significant size reduction and high isolation compared to the traditional CD antennas. The operation principle of the proposed antenna is theoretically analyzed. To validate the presented design concept, two novel DPSD antennas are designed, fabricated, and measured. The first design is a four-port DPSD antenna, which is a straightforward demonstration of the operation principle of the DPSD antenna. The second design is a highly integrated DPSD antenna, which avoids the use of a feed network and provides a simple configuration to design the dual-polarized antenna. Both of the DPSD antennas are designed to operate at 1.7–2.7 GHz for base station applications. The simulated and measured results confirm that the two DPSD antennas have wide bandwidth with VSWR < 1.5 and isolation > 35 dB. In addition, stable gain and half-power beamwidth are obtained with the variance less than ±0.55 dB and ±3.5°, respectively.**

***Index Terms*— Crossed-dipole (CD) antenna, dual-polarized antenna, shared-dipole antenna, wideband antenna.**

I. Introduction

DUAL-POLARIZED antennas have been widely used for wireless communications. Compared with the single-polarized antennas, dual-polarized antennas have the advantages of reducing the multifading effect and increasing the channel capacity [1]. For base station applications, antennas are required for ±45° polarization with wide impedance bandwidth, high isolation, and stable radiation characteristic [2]–[4].

There are many reported designs that use microstrip patch antennas to realize dual polarization. To enhance the impedance bandwidth and isolation, slot coupling [5]–[7] and probe feed techniques [8]–[10] are employed. Modifications to the patches, such as the E-shaped patch [11] and T-shaped slots patch [12], can also improve the operation bandwidth. Recently, electromagnetic coupling [13], tuned loop [14], and filtering resonator feed techniques [15], [16] are developed to obtain wideband and highly isolated dual-polarized antennas. However, due to the low profile and planar structure, microstrip antennas normally have a high-quality factor, and the impedance bandwidth cannot meet the requirement for base station applications.

To increase the impedance bandwidth and improve the stability of the radiation patterns, a popular approach is to use the crossed-dipole (CD) antennas. Crossed hexagonal loop radiator [17] and dual-dipole radiator [18], [19] were reported for base station applications. Another type of the CD antenna is the magnetoelectric dipole (MED) antenna. Simple Γ-shaped strip excited MED antenna [20], differentially driven MED antenna [21], and novel MED antenna [22] were reported. To increase the impedance bandwidth of the antennas, baluns are inserted between the top radiator and the reflector [23]–[25]. However, this method increases the design complexity and the cost of manufacturing. Compact-size dual-polarized antennas are needed for many array antenna systems, such as base stations, radars, and multiple inputs multiple outputs systems. For an array antenna, if the antenna element is half-wavelength long, the distance between the antenna elements is usually much larger than half wavelength, taking consideration of the mutual coupling and isolation. Nevertheless, it is required that the distance between the antenna element should be about a half-wavelength in order to avoid the grating lobes when the array antenna performs beam scanning [29]. Thus, it is necessary to investigate new techniques to reduce the size of dual-polarized antennas.

In this paper, a novel design concept of using shared dipole to design compact dual-polarized antenna is presented. Traditionally, the arms of those reported CD antennas [17], [20]–[25] and dual-dipole antennas [18], [19] for one polarization are not shared for another polarization, and they are separate and independent with a large radiator size. In [18] and [19], four dipoles with eight dipole arms are used for dual polarization separately. On the other hand, in our designs, four-dipole arms are shared for two orthogonal

Manuscript received April 3, 2018; revised July 25, 2018; accepted August 27, 2018. Date of publication September 24, 2018; date of current version November 30, 2018. This work was supported in part by EPSRC under Grant EP/N032497/1 and Grant EP/P015840/1 and in part by the Scholarship from the China Scholarship Council under Grant 201706960013. The work of Q. Wang was supported in part by the Fundamental Research Funds for Central University under Grant JB170106 and in part by the China Postdoctoral Science Foundation under Grant 2016M590924. *(Corresponding author: Le-Hu Wen.)*

L.-H. Wen, S. Gao, and Q. Luo are with the School of Engineering and Digital Arts, University of Kent, Canterbury CT2 7NT, U.K. (e-mail: lw347@kent.ac.uk; s.gao@kent.ac.uk).

C.-X. Mao is with the Department of Electrical Engineering, The Pennsylvania State University, State College, PA 16802 USA.

W. Hu and Y. Yin are with the National Key Laboratory of Antennas and Microwave Technology, Xidian University, Xi'an 710071, China.

Y. Zhou is with the College of Electronic and Information Engineering, Nanjing University of Aeronautics and Astronautics, Nanjing 210016, China.

Q. Wang is with the State Key Laboratory of Integrated Services Network, Xidian University, Xi'an 710071, China.

Color versions of one or more of the figures in this paper are available online at http://ieeexplore.ieee.org.

Digital Object Identifier 10.1109/TAP.2018.2871717

polarizations. Thanks to the shared-dipole configuration, the overall size of the radiator can be theoretically reduced by 50% compared to the traditional dual-polarized CD antennas. Furthermore, the presented dual-polarized shared-dipole (DPSD) antennas have a wideband impedance bandwidth and high isolation which is comparable to the existing designs including the traditional differentially driven dual-polarized CD antennas reported in [3], [17], and [21]. Although the shared-arm dipole linear array is used in [26] and [27] for an imaging radar, the operation principle of the DPSD antenna presented in this paper is completely different. In [26] and [27], each dipole arm is loaded with a large resistor in order to tilt the radiation pattern to broadside direction and increase the impedance bandwidth. Loading resistors to the radiating element would lead to the decrease of the antenna efficiency. Moreover, adding resistors to the radiating element is not a feasible solution to design high-frequency antennas. In this paper, our developed design method achieves broadband operation and high isolation without any resistors loading.

To validate the design concept, two prototypes are designed, fabricated, and measured. One is the four-port DPSD antenna for the conceptual verification, and the other is the highly integrated DPSD antenna for the low-cost design. Both the antennas achieve significant size reductions compared to the CD antennas popularly used for base stations. Furthermore, the operation principle of the proposed DPSD antennas is analyzed and discussed. Both the four-port DPSD antenna and the highly integrated DPSD antenna meet the requirements for the base station systems (1.7–2.7 GHz with VSWR $<$ 1.5 and isolation $>$ 35 dB) with stable gain and half-power beamwidth (HPBW).

II. Operation Principle

In this section, the operation principle of the DPSD antenna is analyzed and discussed. First, the configuration of the DPSD antenna is described and compared to the traditional CD antennas. Then, the isolation and S-parameters for the DPSD antenna are illustrated. The verification of the operation principle of the DPSD antenna and the CD antenna is also investigated.

A. Configuration of the DPSD Antenna

Fig. 1(a) and (b) shows the configurations of the proposed DPSD antennas, which are compared to the traditional CD antennas [Fig. 1(c) and (d)]. A dual-polarized antenna is composed of four arms (Arm1, Arm2, Arm3, and Arm4), and it can be designed as the horizontal and vertical polarizations or the ±45° polarizations. In Fig. 1(a), dipole pair of Arm1 and Arm4 and dipole pair of Arm2 and Arm3 are excited for the horizontal polarization with equal magnitude and co-phase excitation, and dipole pair of Arm1 and Arm2 and dipole pair of Arm3 and Arm4 are excited for the vertical polarization. In Fig. 1(b), a similar method can be applied for ±45° polarizations.

For a dual-polarized antenna, the length of each dipole arm is about $\lambda_0/4$. Different antenna configurations lead to different aperture sizes. The ratios of these different aperture

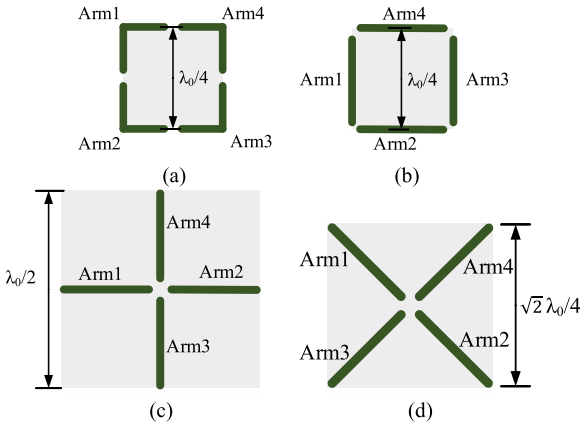

Fig. 1. Different configurations for dual-polarized antenna. (a) ±45° polarized DPSD antenna. (b) Horizontal and vertical polarized DPSD antennas. (c) Horizontal and vertical polarized CD antennas. (d) ±45° polarized CD antenna.

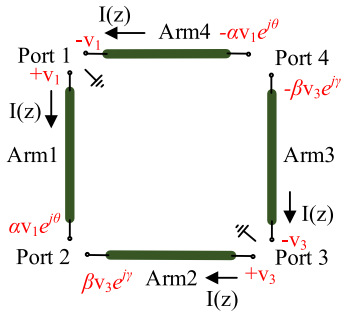

Fig. 2. Equivalent circuit for the DPSD antenna.

sizes are $S_c : S_a = 4 : 1$ and $S_d : S_b = 2 : 1$, where S_a, S_b, S_c, and S_d represent the aperture size of the antenna shown in Fig. 1(a)–(d), respectively. Therefore, the DPSD antenna can effectively reduce the size of the antenna aperture compared to the traditional CD antenna. Theoretically, the DPSD antenna can save 50% of the antenna occupied area compared to a dual-polarized wired CD antenna.

B. Isolation of the DPSD antenna

To explain how the high isolation of the DPSD antenna is achieved, the equivalent circuit for the DPSD antenna is shown in Fig. 2. Assume that the port 1 and port 3 are excited with RF signals with voltage V_{p_1} and V_{p_3}, where

$$\begin{aligned} V_{p_1} &= +v_1 - (-v_1) = 2v_1 \\ V_{p_3} &= +v_3 - (-v_3) = 2v_3. \end{aligned} \tag{1}$$

At the terminal of Arm1, Arm4, Arm2, and Arm3, the voltage values are $\alpha v_1 e^{j\theta}$, $-\alpha v_1 e^{j\theta}$, $\beta v_3 e^{j\gamma}$, and $-\beta v_3 e^{j\gamma}$, respectively, where α and β are the coefficients of the magnitude, and θ and γ are the corresponding delayed phases. Therefore, the voltage values at port 2 and port 4 are

$$\begin{aligned} V_{p_2} &= \alpha v_1 e^{j\theta} - \beta v_3 e^{j\gamma} \\ V_{p_4} &= -\alpha v_1 e^{j\theta} - (-\beta v_3 e^{j\gamma}). \end{aligned} \tag{2}$$

For a symmetrical DPSD antenna, the four arms are of the same length. In addition, port 1 and port 3 excited with equal magnitude and cophase signals. Thus, the following conditions

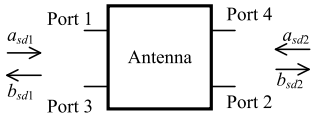

Fig. 3. Four-port single-ended network with common-mode excitation.

should be satisfied:

$$\begin{aligned} v_1 &= v_3 \\ \alpha &= \beta \\ \theta &= \gamma. \end{aligned} \tag{3}$$

Then, it can be derived that

$$V_{p2} = V_{p4} = 0. \tag{4}$$

This means that if port 1 and port 3 are excited with equal magnitude and cophase signals, the voltage across the other two ports (port 2 and port 4) is zero. For the DPSD antenna, the signals transmitted from port 1 to port 3 are canceled by each other at port 2 and port 4. Therefore, high isolation is obtained for the DPSD antenna.

C. S-Parameters of the DPSD antenna

Each polarization of the DPSD antenna needs two equal magnitude and cophase excitations, and normally it needs a feed network. To facilitate the evaluation of antenna performance without using a feed network, the S-parameters are analyzed by using the principle of four-port microwave network theory [28].

Four-port excited DPSD antenna is regarded as a common-mode excited four-port network. Fig. 3 shows the equivalent four-port single-ended network with common-mode excitation. Single-ended port 1 and port 3 are together designated as shared-dipole port 1 for one polarization, and single-ended port 2 and port 4 are together defined as shared-dipole port 2 for another polarization. The S-parameters for the DPSD antenna (S_{sd11}, S_{sd22}, S_{sd21}, and S_{sd12}) are derived as

$$\begin{aligned} S_{sd} &= \begin{bmatrix} S_{sd11} & S_{sd12} \\ S_{sd21} & S_{sd22} \end{bmatrix} = \begin{bmatrix} \dfrac{b_{sd1}}{a_{sd1}} & \dfrac{b_{sd1}}{a_{sd2}} \\ \dfrac{b_{sd2}}{a_{sd1}} & \dfrac{b_{sd2}}{a_{sd2}} \end{bmatrix} \\ &= \frac{1}{2} \begin{bmatrix} S_{11}+S_{13}+S_{31}+S_{33} & S_{12}+S_{14}+S_{32}+S_{34} \\ S_{21}+S_{23}+S_{41}+S_{43} & S_{22}+S_{24}+S_{42}+S_{44} \end{bmatrix}. \end{aligned} \tag{5}$$

As expressed in (5), the S-parameters of the DPSD antenna are calculated by taking the mutual couplings into consideration. Thus, the input impedance and VSWR of the DPSD antenna can be calculated as

$$Z_{sd11} = Z_0 \frac{1+S_{sd11}}{1-S_{sd11}} \tag{6}$$

$$\mathrm{VSWR}_{sd} = \frac{1+|S_{sd11}|}{1-|S_{sd11}|}. \tag{7}$$

By using (5)–(7), the actual impedance and isolation bandwidth for the DPSD antenna are derived. This method enables the verification of the S-parameters of the DPSD antenna without using any external power divider network.

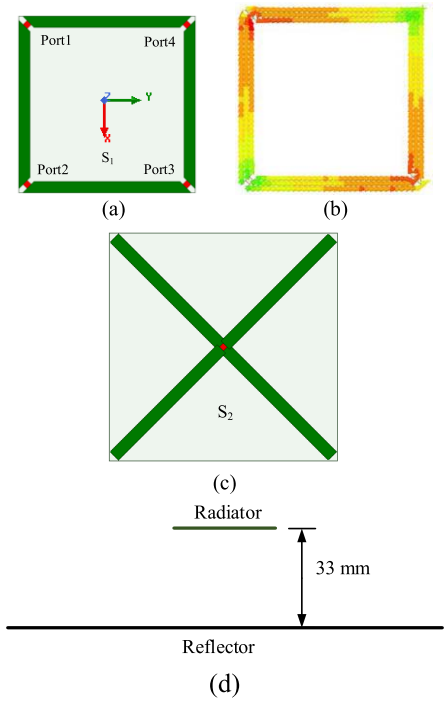

Fig. 4. Models of simulated DPSD antenna. (a) DPSD antenna. (b) Surface current distribution of DPSD antenna with port 1 and port 3 excited. (c) CD antenna. (d) Side view of both two simulated antenna models.

D. Comparison Between the DPSD and CD Antennas

To verify the above-mentioned analysis, both the DPSD antenna and the CD antenna are simulated by using ANSYS Electromagnetics Suite 18. Both antennas are arranged for ±45° polarizations. The two antennas are excited with ideal lumped ports. As a general definition in this paper, the *yz* plane is designated as the horizontal plane (H-plane), and the *xz* plane is defined as the vertical plane (V-plane).

As shown in Fig. 4, the width of the dipole arm for the DPSD antenna and the CD antenna is 2 mm. The distance from the radiator to the reflector for both antennas is 33 mm. The two dual-polarized antennas are designed at the resonant frequency of 2.5 GHz. The length of each antenna arm is about a quarter wavelength in free space. Fig. 4(b) shows the surface current distribution when port 1 and port 3 are excited with equal magnitude and cophase signals. As can be seen, the strongest current magnitude is in the center of the feed point, and the weakest current magnitude is at the end of the dipole arm, which implies good isolation is obtained for another polarization.

Fig. 5 shows the input impedance of the DPSD antenna (Z_{sd11}) and the CD antenna (Z_{cd11}). The real parts of the input impedance of the two antennas are almost the same. Regarding the imaginary part, the DPSD antenna has a flatter variation than that of the CD antenna, which means a wider impedance bandwidth can be achieved for the DPSD antenna.

Fig. 6 compares the simulated normalized H-plane radiation patterns between the DPSD antenna and the CD antenna when port 1 and port 3 are excited with the ideal equal magnitude and cophase signal. The radiation patterns are almost the same in the range of ±30° around the boresight direction. In the

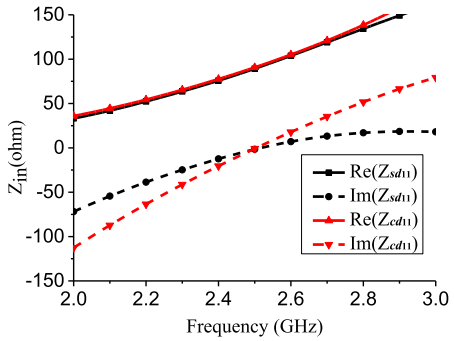

Fig. 5. Input impedance of the DPSD antenna and the CD antenna.

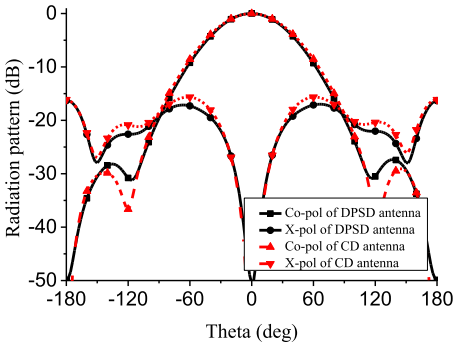

Fig. 6. H-plane radiation patterns of the DPSD antenna and the CD antenna.

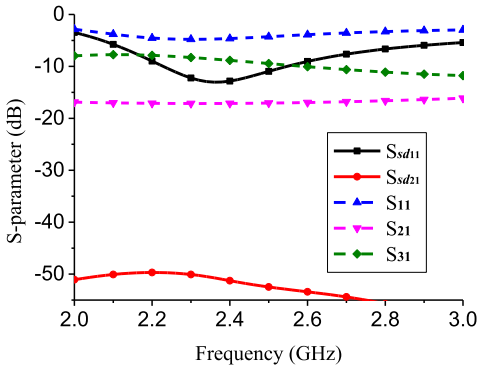

Fig. 7. Simulated S-parameters of the DPSD antenna.

range of ±90°, the DPSD antenna has slightly lower cross polarization discrimination (XPD) than the CD antenna.

The simulated S-parameters of the four-port DPSD antenna are shown in Fig. 7. The isolation between port 1 and port 3 (S_{31}) is about −10 dB and the isolation between port 1 and port 2 (S_{21}) is about −17 dB. As discussed in Section II-C, (5) needs to be used for S-parameters calculation. The calculated results are also shown in Fig. 7. The best impedance matching frequency for the DPSD antenna is at about 2.4 GHz, and the isolation is better than 50 dB.

III. Design I: Four-Port DPSD Antenna

In this section, the configuration of the four-port DPSD antenna is illustrated. Then, the presented antenna is analyzed and discussed using its equivalent circuit model. Then, the prototype of the four-port DPSD antenna is fabricated and measured by two methods.

A. Antenna Structure

The configuration of the four-port DPSD antenna is shown in Fig. 8. The developed antenna is composed of a radiator,

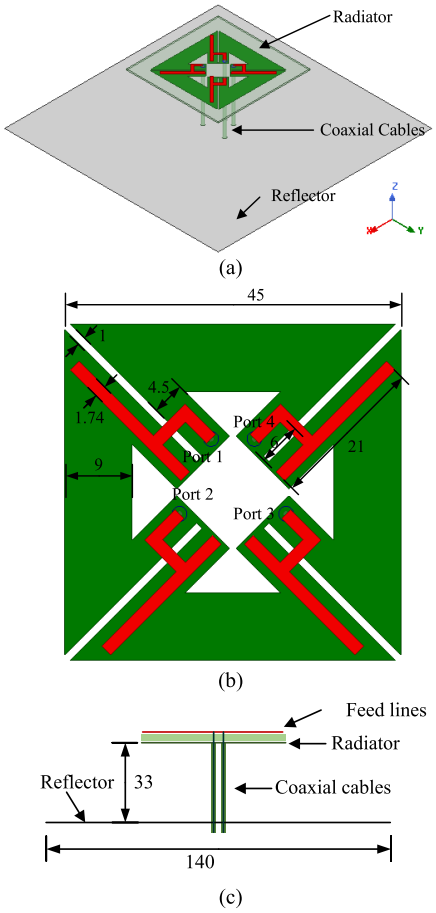

Fig. 8. Geometry of the four-port DPSD antenna. (a) 3-D view. (b) Detailed configuration of radiator. (c) Side view (unit: mm).

four equal-length semiflexible coaxial cables, and a reflector for unidirectional radiation. Rogers RO4003C substrates with a relative dielectric constant of 3.55 and thickness of 0.813 mm are employed for the antenna design. The bottom layer of the substrate is four symmetrically arranged shared-dipole arms connected by four shorted coplanar striplines (CPSs). The top layer is the four feed lines, which is designed for the antenna impedance matching. The CPS on the bottom layer and the feed line on the top layer together function as a balun, which transforms the unbalanced coaxial line to the balanced CPS. The outer conductor of the coaxial cable is soldered to the bottom layer of CPS, while the inner conductor of the coaxial cable is soldered to the top layer of the feed line. Fig. 8(c) depicts the side view of the four-port DPSD antenna. The distance from the radiator to the reflector is 33 mm, which is about a quarter wavelength at 2.2 GHz in the free space. The size of the square reflector is 140 mm × 140 mm.

B. Antenna Analysis

Fig. 9 shows the equivalent circuit model of the four-port DPSD antenna. The single-ended unbalanced coaxial cables are connected to the baluns; then, the unbalanced coaxial cables are transformed into the balanced CPSs. By using the balanced CPSs feed method, four shared-dipole arms are excited for the balanced radiation.

Fig. 10 illustrates the design steps of the proposed four-port DPSD antenna. The corresponding simulated S-parameters

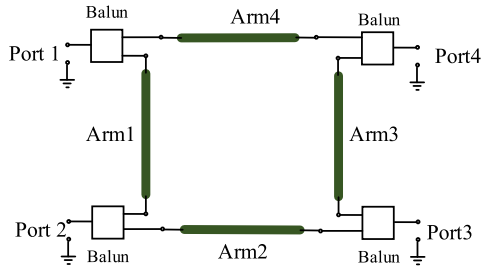

Fig. 9. Equivalent circuit model of the four-port DPSD Antenna.

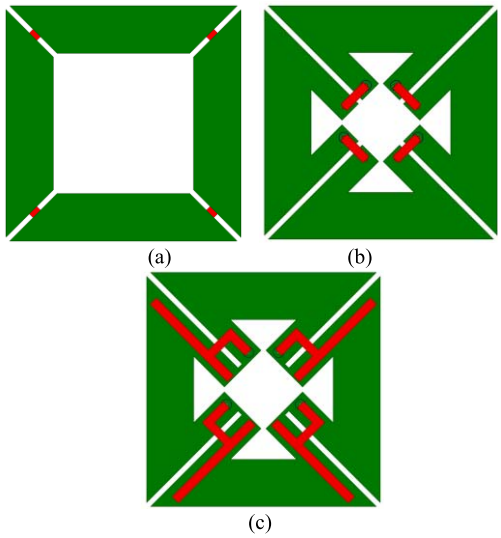

Fig. 10. Design steps of the four-port DPSD antenna. (a) With ideal lumped port feed. (b) With CPS feed. (c) With balun feed.

under different design steps are shown in Fig. 11. First, the four-port DPSD antenna is excited with four ideal 50 Ω lumped ports. One resonance can be founded at about 2 GHz, and the isolation is better than 60 dB. When the four-port DPSD antenna is fed by CPS connected by a 50 Ω coaxial cable, a better impedance matching is obtained, but the isolation at higher frequency band is deteriorated because of the unbalanced feed coaxial cables. To realize the balanced feed and increase the impedance bandwidth, y-shaped open feed line and shorted CPS are employed to form a balun. As a result, another resonance is obtained and the impedance bandwidth is increased. Moreover, the isolation within the whole frequency band is higher than 48 dB.

C. Results and Discussion

To validate the operation principle and the analysis of the four-port DPSD antenna, the proposed antenna is verified by two measurement methods, one is measured directly without feed network, and the other is measured with feed network.

1) Without Feed Network: Fig. 12 shows the photographs of the fabricated four-port DPSD antenna. The antenna is fed by four semiflexible coaxial cables. Fig. 13 shows the simulated and measured four-port single-ended S-parameters. Due to the symmetry of the antenna, only the simulated and measured S_{11}, S_{22}, S_{21}, S_{31}, and S_{41} are shown in Fig. 13. The measured S-parameters agree well with the simulated results. The small discrepancy is mainly due to the effect of

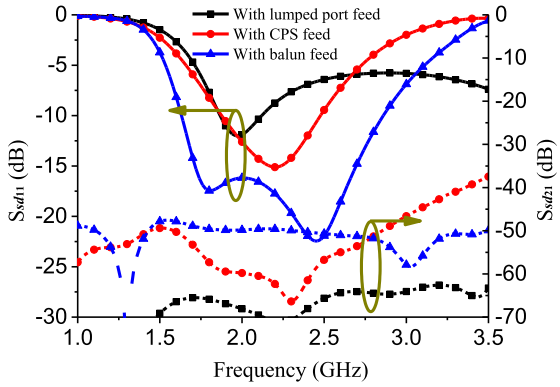

Fig. 11. Simulated S-parameters of the four-port DPSD antenna with different feed methods.

Fig. 12. Photographs of the fabricated four-port DPSD antenna without feed network. (a) Top view. (b) Side view.

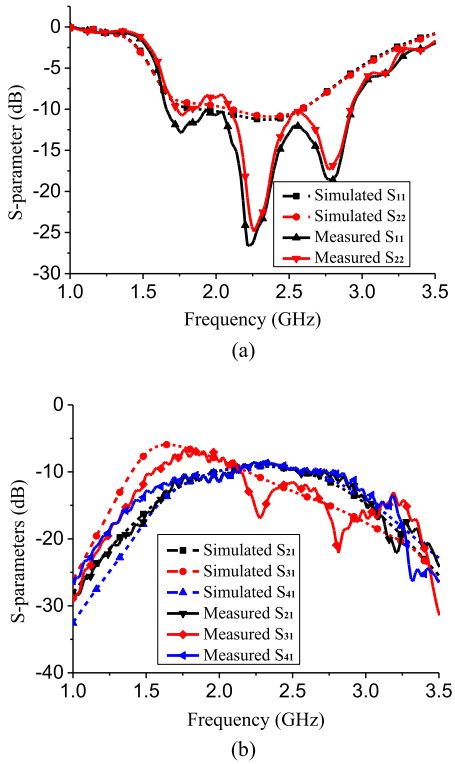

Fig. 13. Simulated and measured S-parameters for the four-port DPSD antenna. (a) S_{11} and S_{22}. (b) S_{21}, S_{31}, and S_{41}.

the extension of the coaxial cables and the fabrication errors of the antenna.

To illustrate the true impedance characteristic of the DPSD antenna, by using (5)–(7), the calculated VSWR and isolation from the simulated and measured four-port S-parameters are shown in Fig. 14. The calculated overlapped impedance bandwidth for VSWR < 1.5 of the dual polarization is from

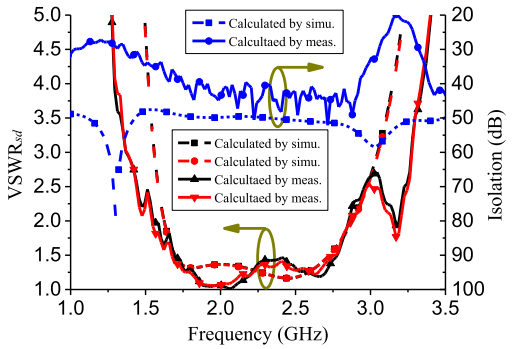

Fig. 14. Calculated VSWR and isolation by the simulated and measured results for the four-port DPSD antenna without feed network.

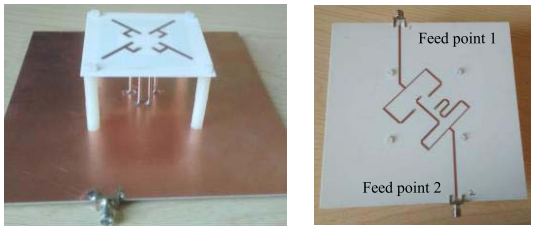

Fig. 15. Photographs of the fabricated four-port DPSD antenna with the feed network. (a) Antenna radiator and reflector. (b) Feed network on the bottom layer of the reflector.

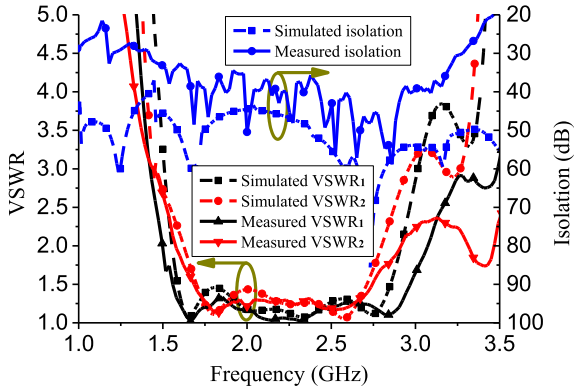

Fig. 16. Simulated and measured results for the four-port DPSD antenna with the feed network.

1.69 to 2.77 GHz. Although the measured isolation is slightly lower than the simulated isolation, it is still better than 37 dB within the impedance bandwidth.

2) With Feed Network: As discussed in Section II, the four-port DPSD antenna needs equal magnitude and cophase excitation. Therefore, a feed network is designed to feed the four-port DPSD antenna. The photograph of the four-port DPSD antenna with the feed network is shown in Fig. 15. The reflector of the antenna is replaced by a PCB with one layer of copper functioned as a reflector and the other layer composed of the antenna feed network. The four output ports of the power dividers are connected to the four input ports of the antenna radiator by four semiflexible coaxial cables with equal length and phase. Each input port of the power divider is connected by an SMA connector for each polarization.

Fig. 16 shows the simulated and measured VSWR and isolation at the two ends of the feed network. A good agreement is observed between the simulated and measured results.

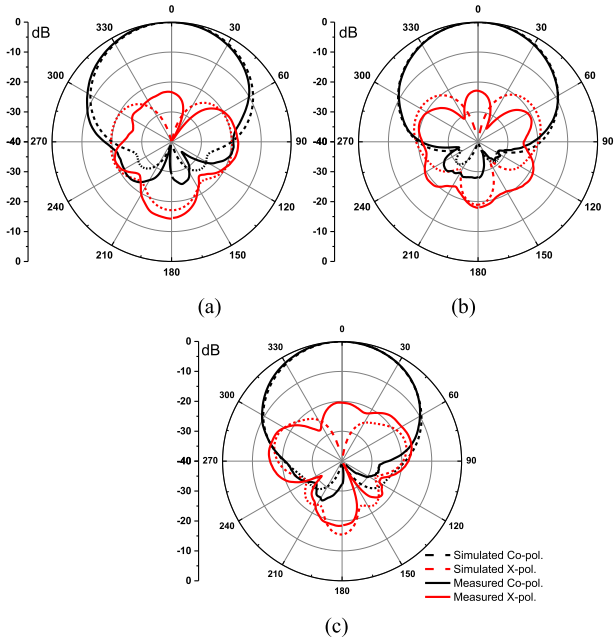

Fig. 17. Simulated and measured radiation patterns of the four-port DPSD antenna with the feed network for the H-plane when the feed point 1 excited. (a) 1.7 GHz. (b) 2.2 GHz. (c) 2.7 GHz.

Due to the effect of the feed network, the impedance bandwidth for port 1 is slightly wider than port 2. The measured overlapped two-port impedance bandwidth for VSWR < 1.5 is from 1.68 to 2.74 GHz. The isolation of the impedance bandwidth is better than 35 dB, which is close to the calculated isolation of the four-port DPSD antenna using (5)–(7).

The measured and simulated H-plane radiation patterns of the four-port DPSD antenna with the feed network when feed point 1 is excited are shown in Fig. 17. Because of the symmetrical configuration, only the radiation patterns at 1.7, 2.2, and 2.7 GHz are presented. The measured XPD at boresight direction is better than 20 dB over 1.7–2.7 GHz. For the direction over the range of $\pm 30°$, the XPD is better than 20 dB. Fig. 18 shows the simulated and measured gain and HPBW within the bandwidth of the antenna. There is a good agreement between the measured and simulated results, which shows stable gain and HPBW are obtained. The measured gain varies from 7.1 to 8.2 dBi, and the measured HPBW for H-plane varies from 66° to 71°.

IV. Design II: Highly Integrated DPSD Antenna

In this section, a highly integrated DPSD antenna, which avoids using the feed network, is put forward with only two single-ended feed coaxial cables. An equivalent circuit of this proposed antenna is illustrated. Finally, the proposed highly integrated DPSD antenna is fabricated and measured for verification.

A. Antenna Structure

The configuration of the highly integrated DPSD antenna is shown in Fig. 19. The proposed antenna consists of three parts, the radiator for dual polarization, two coaxial cables for direct feed, and a square reflector. Compared to the four-port prototype in Section III, this antenna is integrated with two pairs of CPSs, and two coaxial cables are soldered on each pair of

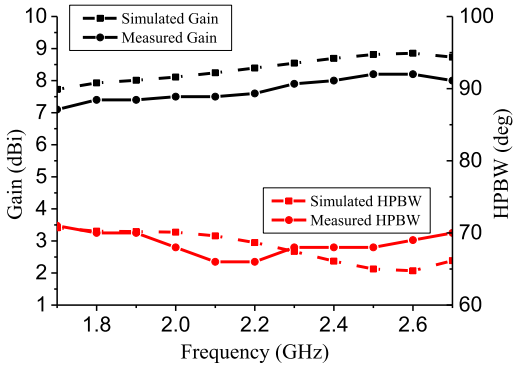

Fig. 18. Simulated and measured gain and HPBW for H-plane when the feed point 1 excited.

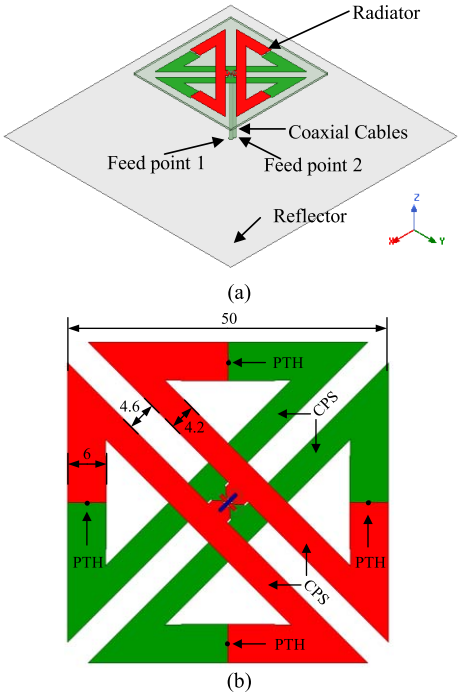

Fig. 19. Geometry of the highly integrated DPSD Antenna. (a) 3-D view. (b) Top view of the radiator (unit: mm).

the CPS for each polarization. This direct coax feed method avoids the use of the feed network and thus reduces the design complexity and fabrication cost. The antenna is printed on a substrate of Rogers RO4003C substrates with a relative dielectric constant of 3.55 and thickness of 0.813 mm.

As shown in Fig. 19(b), the top layer of the antenna is depicted in red color, while the bottom layer is highlighted in green color. Four plated through holes are inserted into the dipole arms to connect the radiating element. At the center of the PCB, two coaxial cables are connected to the crossed CPSs for each polarization. Specifically, for the $+45°$ polarization, the outer conductor of one coaxial cable is soldered on the top right side of the CPS, and the inner conductor is soldered on the bottom left side of the CPS. Same feed method is applied to the $-45°$ polarization. The distance from the radiator to the radiator is 33 mm and the square reflector size is 140 mm.

B. Antenna Analysis

Fig. 20 shows the equivalent circuit of the highly integrated DPSD antenna. The characteristic impedance of the CPS is Z_1,

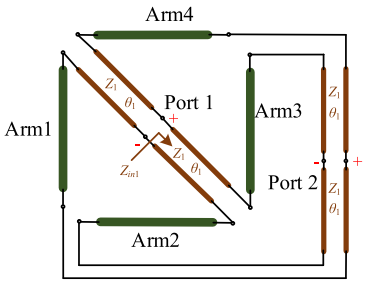

Fig. 20. Equivalent circuit of highly integrated DPSD antenna.

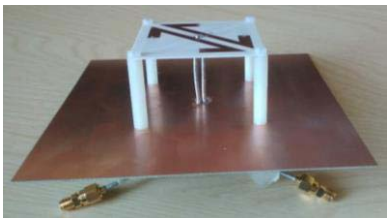

Fig. 21. Photograph of the fabricated highly integrated DPSD antenna.

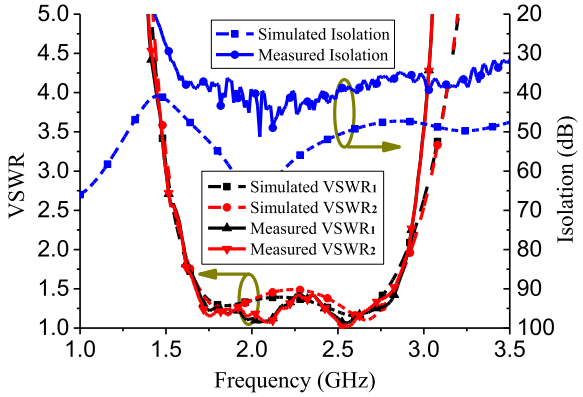

Fig. 22. Simulated and measured results for the highly integrated DPSD antenna.

and its phaselength is θ_1. Therefore, the input impedance Z_{in1} is

$$Z_{in1} = Z_1 \frac{2Z_{sd11} + jZ_1 \tan\theta_1}{Z_1 + j2Z_{sd11}\tan\theta_1}. \tag{8}$$

Then, the input impedance at port 1 is

$$Z_{in} = \frac{Z_{in1}}{2} = \frac{Z_1}{2} \frac{2Z_{sd11} + jZ_1 \tan\theta_1}{Z_1 + j2Z_{sd11}\tan\theta_1}. \tag{9}$$

Therefore, if $\theta_1 = 90°$, the transmission line (Z_1) acts as an impedance transformer. In this condition, it can be derived that

$$Z_{in} = \frac{Z_1^2}{4Z_{sd11}}. \tag{10}$$

Thus, (8)–(10) provide a good guidance to design the highly integrated DPSD antenna.

C. Results and Discussion

Based on the above-mentioned analysis, the highly integrated DPSD antenna is fabricated and measured. Fig. 21 shows the photograph of the highly integrated DPSD antenna. Fig. 22 shows the simulated and measured VSWR and isolation for the highly integrated DPSD antenna. The measured overlapped impedance bandwidth for VSWR < 1.5

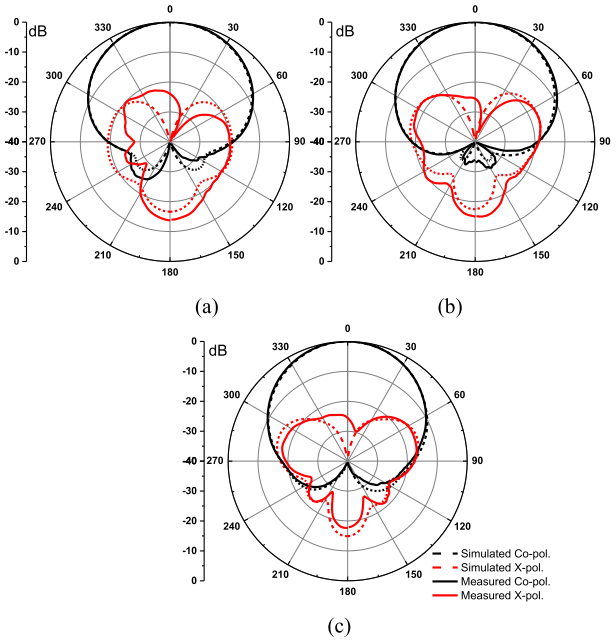

Fig. 23. Simulated and measured radiation patterns of the highly integrated DPSD antenna for the H-plane with the feed point 1 excited. (a) 1.7 GHz. (b) 2.2 GHz. (c) 2.7 GHz.

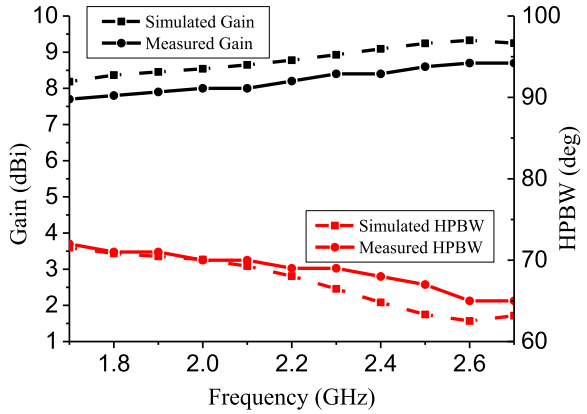

Fig. 24. Simulated and measured gains and HPBW of the highly integrated DPSD antenna for H-plane with feed point 1 excited.

is from 1.69 to 2.82 GHz, and the corresponding isolation is better than 36 dB. Both the simulated and measured radiation patterns at 1.7, 2.2, and 2.7 GHz are shown in Fig. 23 for comparison. The measured XPD is over 23 dB at the boresight direction, and better than 22 dB over the range of ±30° direction. In Fig. 24, the measured average gain is about 8.2 dBi (7.7–8.7 dBi) and the HPBW is about 68° (65°–72°) for the base station frequency band.

Compared to the four-port DPSD antenna, the XPD and gain of the integrated DPSD antenna are a little bit higher, while the impedance characteristic and isolation are almost the same. Furthermore, the proposed highly integrated DPSD antenna only needs two single-ended coaxial cables for dual polarization as the traditional dual-polarized antenna. It reduces the manufacturing cost with the integrated feed CPSs on the radiating element. With a simple configuration and good radiation performances, it is suitable for the low-cost base station applications.

TABLE I
COMPARISON OF THE DUAL-POLARIZED ANTENNAS FOR BASE STATIONS

Antennas	Radiator size (mm×mm)	Height (mm)	VSWR / RL for base station	Isolation (dB)
[2]	140×140	41	VSWR<1.5	>25
[3]	109.8×109.8	55	VSWR<1.5	>39
[17]	68.5×68.5	34	VSWR<1.5	>26
[18]	68×68	42	RL>15 dB	>30
[22]	61.6×61.6	45.7	VSWR<1.5	>30
[24]	70.4×70.4	27	RL>15 dB	>28
Antenna 1	45×45	33	VSWR<1.5	>35
Antenna 2	50×50	33	VSWR<1.5	>36

Table I compares the developed antennas with the CD antennas reported in recently published papers that can operate from 1.7 to 2.7 GHz for base station applications. Antenna 1 is the prototype DPSD antenna with the feed network in this paper, and antenna 2 is the highly integrated DPSD antenna. Antennas in [2], [18], [22], and [24] are the traditional CD antennas. In [2], four parasitic elements are inserted beside the CDs to enhance the XPD of the dual-polarized antenna; however, this method increases the overall size of the antenna. It should be noted that antennas in [3] and [17] are the typical differentially driven dual-polarized CD antennas, which is known for their ideal high isolation. The proposed DPSD antennas are of the similar high isolation as the differentially driven antennas but with more compact size. Compared to these antennas, the proposed DPSD antennas have the most compact size with very high isolation.

V. CONCLUSION

This paper presents a novel design method which uses shared dipole to design a wideband and high isolated dual-polarized antenna. Operation principles including isolation and S-parameters are analyzed and discussed. To validate the design concept, two DPSD antenna prototypes are implemented and measured. One is the four-port DPSD antenna for conceptual verification and the other is the highly integrated DPSD antenna for low-cost configuration. Both the simulated and measured results show that the two DPSD antennas have a broad bandwidth from 1.7 to 2.7 GHz with VSWR $<$ 1.5 and isolation $>$ 35 dB. Stable radiation performances in terms of the antenna gain and HPBW are obtained for base station applications. The variation of the measured gain and HPBW for the four-port DPSD antenna and the highly integrated DPSD antenna is no more than ±0.55 dB and ±3.5°, respectively. Compared with the traditional CD antennas, the proposed DPSD antennas have the similar high isolation as the differential driven CD antenna with a more compact size. The presented design method is flexible and can be applied to the design of other dual-polarized antennas operating at other frequencies.

REFERENCES

[1] P. K. Mishra, D. R. Jahagirda, and G. Kumar, "A review of broadband dual linearly polarized microstrip antenna designs with high isolation [education column]," *IEEE Antennas Propag. Mag.*, vol. 56, no. 6, pp. 238–251, Dec. 2014.

[2] Y. Luo, Q.-X. Chu, and D.-L. Wen, "A plus/minus 45 degree dual-polarized base-station antenna with enhanced cross-polarization discrimination via addition of four parasitic elements placed in a square contour," *IEEE Trans. Antennas Propag.*, vol. 64, no. 4, pp. 1514–1519, Apr. 2016.
[3] Y. Luo and Q.-X. Chu, "Oriental crown-shaped differentially fed dual-polarized multidipole antenna," *IEEE Trans. Antennas Propag.*, vol. 63, no. 11, pp. 4678–4685, Nov. 2015.
[4] C. Ding, H. Sun, R. W. Ziolkowski, and Y. J. Guo, "Simplified tightly-coupled cross-dipole arrangement for base station applications," *IEEE Access*, vol. 5, pp. 27491–27503, 2017.
[5] S.-C. Gao, L.-W. Li, M.-S. Leong, and T.-S. Yeo, "Dual-polarized slot-coupled planar antenna with wide bandwidth," *IEEE Trans. Antennas Propag.*, vol. 51, no. 3, pp. 441–448, Mar. 2003.
[6] Y. Wang and Z. Du, "Dual-polarized slot-coupled microstrip antenna array with stable active element pattern," *IEEE Trans. Antennas Propag.*, vol. 63, no. 9, pp. 4239–4244, Sep. 2015.
[7] S. Gao, L. W. Li, M. S. Leong, and T. S. Yeo, "A broad-band dual-polarized microstrip patch antenna with aperture coupling," *IEEE Trans. Antennas Propag.*, vol. 51, no. 4, pp. 898–900, Apr. 2003.
[8] H.-W. Lai and K.-M. Luk, "Dual polarized patch antenna fed by meandering probes," *IEEE Trans. Antennas Propag.*, vol. 55, no. 9, pp. 2625–2627, Sep. 2007.
[9] Y.-X. Guo, K.-W. Khoo, and L. C. Ong, "Wideband dual-polarized patch antenna with broadband baluns," *IEEE Trans. Antennas Propag.*, vol. 55, no. 1, pp. 78–83, Jan. 2007.
[10] W. Qiu, C. Chen, H. Zhang, and W. Chen, "A wideband dual-polarized L-probe antenna array with hollow structure and modified ground plane for isolation enhancement," *IEEE Antennas Wireless Propag. Lett.*, vol. 16, pp. 2820–2823, 2017.
[11] Y. Gou, S. Yang, Q. Zhu, and Z. Nie, "A compact dual-polarized double E-shaped patch antenna with high isolation," *IEEE Trans. Antennas Propag.*, vol. 61, no. 8, pp. 4349–4353, Aug. 2013.
[12] B. Li, Y.-Z. Yin, W. Hu, Y. Ding, and Y. Zhao, "Wideband dual-polarized patch antenna with low cross polarization and high isolation," *IEEE Antennas Wireless Propag. Lett.*, vol. 11, pp. 427–430, 2012.
[13] J.-J. Xie, X.-S. Ren, Y.-Z. Yin, and J. Ren, "Dual-polarised patch antenna with wide bandwidth using electromagnetic feeds," *Electron. Lett.*, vol. 48, no. 22, pp. 1385–1386, 2012.
[14] J. Y. Deng, L. X. Guo, Y. Z. Yin, J. Qiu, and Z. S. Wu, "Broadband patch antennas fed by novel tuned loop," *IEEE Trans. Antennas Propag.*, vol. 61, no. 4, pp. 2290–2293, Apr. 2013.
[15] C.-X. Mao, S. Gao, Y. Wang, F. Qin, and Q.-X. Chu, "Multimode resonator-fed dual-polarized antenna array with enhanced bandwidth and selectivity," *IEEE Trans. Antennas Propag.*, vol. 63, no. 12, pp. 5492–5499, Dec. 2015.
[16] C.-X. Mao, S. Gao, Y. Wang, Q. Luo, and Q.-X. Chu, "A shared-aperture dual-band dual-polarized filtering-antenna-array with improved frequency response," *IEEE Trans. Antennas Propag.*, vol. 65, no. 4, pp. 1836–1844, Apr. 2017.
[17] D.-L. Wen, D.-Z. Dong, and Q.-X. Chu, "A wideband differentially fed dual-polarized antenna with stable radiation pattern for base stations," *IEEE Trans. Antennas Propag.*, vol. 65, no. 5, pp. 2248–2255, May 2017.
[18] Y. Cui, X. Gao, H. Fu, Q.-X. Chu, and R. Li, "Broadband dual-polarized dual-dipole planar antennas: Analysis, design, and application for base stations," *IEEE Antennas Propag. Mag.*, vol. 59, no. 6, pp. 77–87, Dec. 2017.
[19] Y. Cui, X. Gao, and R. Li, "A broadband differentially fed dual-polarized planar antenna," *IEEE Trans. Antennas Propag.*, vol. 65, no. 6, pp. 3231–3234, Jun. 2017.
[20] B. Q. Wu and K. M. Luk, "A broadband dual-polarized magneto-electric dipole antenna with simple feeds," *IEEE Antennas Wireless Propag. Lett.*, vol. 8, pp. 60–63, 2009.
[21] Q. Xue, S. W. Liao, and J. H. Xu, "A differentially-driven dual-polarized magneto-electric dipole antenna," *IEEE Trans. Antennas Propag.*, vol. 61, no. 1, pp. 425–430, Jan. 2013.
[22] S.-G. Zhou, Z.-H. Peng, G.-L. Huang, and C.-Y.-D. Sim, "Design of a novel wideband and dual-polarized magnetoelectric dipole antenna," *IEEE Trans. Antennas Propag.*, vol. 65, no. 5, pp. 2645–2649, May 2017.
[23] Y. Gou, S. Yang, J. Li, and Z. Nie, "A compact dual-polarized printed dipole antenna with high isolation for wideband base station applications," *IEEE Trans. Antennas Propag.*, vol. 62, no. 8, pp. 4392–4395, Aug. 2014.
[24] H. Sun, C. Ding, B. Jones, and Y. J. Guo, "A wideband base station antenna element with stable radiation pattern and reduced beam squint," *IEEE Access*, vol. 5, pp. 23022–23031, 2017.
[25] H. Zhai, Y. Zang, and L. Li, "A low-profile dual-polarized high-isolation MIMO antenna arrays for wideband base-station applications," *IEEE Trans. Antennas Propag.*, vol. 66, no. 1, pp. 191–202, Jan. 2018.
[26] W. Kang, D. W. Yang, and K. Kim, "Design of shared-arm dipole array for imaging radar applications," *Electron. Lett.*, vol. 48, no. 15, pp. 951–953, 2012.
[27] W. Kang, K. Kim, and W. Kim, "Design of a 16-port shared-arm dipole array for monostatic imaging radar," *IEEE Trans. Antennas Propag.*, vol. 62, no. 1, pp. 454–459, Jan. 2014.
[28] W. Fan, A. Lu, L. L. Wai, and B. K. Lok, "Mixed-mode S-parameter characterization of differential structures," in *Proc. 5th Electron. Packag. Technol. Conf. (EPTC)*, Dec. 2003, pp. 533–537.
[29] C. A. Balanis, *Antenna Theory: Analysis and Design*, 3rd ed. New York, NY, USA: Wiley, 2005.
[30] L.-H. Wen *et al.*, "A wideband dual-polarized antenna using shorted dipoles," *IEEE Access*, vol. 6, pp. 39725–39733, 2018.

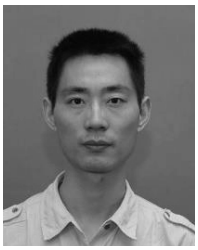

Le-Hu Wen received the M.S. degree in Xidian University, Xi'an, China, in 2011. He is currently pursuing the Ph.D. degree with the University of Kent, Canterbury, U.K.

His current research interests include multiband base station antenna, mobile terminal antenna, and tightly coupled array.

Steven Gao (M'01–SM'16) received the Ph.D. degree in microwave engineering from Shanghai University, Shanghai, China, in 1999.

He is currently a Professor and the Chair of RF and microwave engineering with the University of Kent, Canterbury, U.K. His current research interests include smart antennas, phased arrays, MIMO, satellite antennas, satellite communications, UWB radars, synthetic aperture radars, and mobile communications.

Dr. Gao is an Associate Editor of the IEEE TRANSACTIONS ON ANTENNAS AND PROPAGATION.

Qi Luo (S'08–M'12) is currently a Research Associate with the School of Engineering and Digital Arts, University of Kent, Canterbury, U.K.

Chun-Xu Mao (M'18) is currently a Post-Doctoral Research Associate with the Computational Electromagnetics and Antennas Research Laboratory, Department of Electrical Engineering, The Pennsylvania State University, State College, PA, USA.

Wei Hu (S'09–M'14) is currently an Associate Professor with the National Key Laboratory of Antennas and Microwave Technology, Xidian University, Xi'an, China.

Yingzeng Yin (M'16) is currently a Professor with the National Key Laboratory of Antennas and Microwave Technology, Xidian University, Xi'an, China.

Yonggang Zhou is currently an Associate Professor with the College of Electronic and Information Engineering, Nanjing University of Aeronautics and Astronautics, Nanjing, China.

Qiwei Wang is currently a Lecturer with the State Key Laboratory of Integrated Services Network, Xidian University, Xi'an, China.